Journal of Alloys and Compounds 791 (2019) 477–482

Contents lists available at ScienceDirect

Journal of Alloys and Compounds

journal homepage: http://www.elsevier.com/locate/jalcom

Investigation of $Zr_{55}Cu_{30}Al_{10}Ni_5$ bulk amorphous alloy crystallization

Ruslan A. Sergiienko [a, b, *], Oleksandr A. Shcheretskyi [a], Vladislav Yu. Zadorozhnyy [b, c], Anatolii M. Verkhovliuk [a], Dmitri V. Louzguine-Luzgin [d, e]

[a] Physico-Technological Institute of Metals and Alloys, National Academy of Sciences of Ukraine, 34/1, Vernadsky Ave., Kyiv-142, 03680, Ukraine
[b] National University of Science and Technology «MISiS», 119049, Leninsky pr.4, Moscow, Russia
[c] Erich Schmid Institute of Materials Science, Austrian Academy of Sciences, Leoben, 8700, Austria
[d] WPI Advanced Institute for Materials Research, Tohoku University, Katahira 2-1-1, Aoba-ku, Sendai, 980-8577, Japan
[e] Mathematics for Advanced Materials-OIL, National Institute of Advanced Industrial Science and Technology (AIST), Sendai 980-8577, Japan

ARTICLE INFO

Article history:
Received 17 February 2019
Received in revised form
18 March 2019
Accepted 19 March 2019
Available online 22 March 2019

Keywords:
Metallic glasses
Amorphous materials
Crystal structure
Differential scanning calorimetry
Dynamic mechanical analysis

ABSTRACT

The process of transition of the $Zr_{55}Cu_{30}Al_{10}Ni_5$ bulk amorphous alloy from an amorphous into a crystalline state has been investigated by using differential scanning calorimetry and dynamic mechanical analysis. The parameters of crystallization of the alloy, such as glass transition temperature (T_g), crystallization temperature (T_x), activation energy of crystallization (E_a), solidus and liquidus temperatures (T_{sol}, T_{liq}), crystallization enthalpy (ΔH_x), melting heat (ΔH_m) and solidification heat (ΔH_{sol}) have been determined. The behavior of the storage modulus (E^I), the loss factor ($\tan\delta$) with a temperature change from room temperature to 873 K has been studied. The phase structure of the alloy after crystallization was investigated by using X-ray diffraction.

1. Introduction

Currently, the bulk metallic glasses (BMGs) (or bulk glassy alloys, bulk amorphous alloys) attract increased interest due to their unique physical-mechanical properties such as high hardness, large elastic deformation and high fatigue strength, as well as increased wear resistance and corrosion resistance [1,2]. The Zr-based alloys have a higher glass-forming ability compared to other alloy systems (e.g. Cu-, Ni-, Fe-, Co-, Ti-, Mg, Al-based glassy alloys). The bulk amorphous alloys with critical diameter of over 30 mm have been made from zirconium with other transition and nontransition metals [1,3]. In connection with the promising practical application of the bulk amorphous alloys the structure and mechanical properties of different glassy alloy systems such as Zr-Cu-Ni, Zr-Cu-Ni-Al, Zr-Cu-Ni-Al-Ti, Zr-Cu-Ni-Al-Nb, Zr-Cu-Ni-Al-Pd were studied in a number of works [4–7]. Also, a Zr-based nanostructured material with improved mechanical properties obtained after a heat treatment of a bulk amorphous alloy is a promising candidate for implants in the treatment of bone fractures [8].

The aim of this work was to study the transition process of the $Zr_{55}Cu_{30}Al_{10}Ni_5$ bulk amorphous alloy from an amorphous into a crystalline state using differential scanning calorimetry (DSC) and dynamic mechanical analysis (DMA). With DMA it is possible to investigate the material response (deformation, phase shift, amplitude, and stress) and to make a quantitative determination of the mechanical properties of a sample under an oscillating load and as a function of temperature, time and frequency [9]. As a result, the complex elasticity modulus of a viscoelastic material can be deduced from dynamic mechanical analysis, which can be written in the following form:

$$|E| = \sqrt{\left[E^I(\omega)\right]^2 + \left[E^{II}(\omega)\right]^2} \quad (1)$$

where E^I – the storage modulus (Young's modulus) is an elastic component that characterizes the elastic properties of the material; E^{II} – the loss modulus is a viscoelastic component that characterizes the conversion of mechanical energy into other forms of energy, such as heat and E^{II} is a measure of the unreturned, lost oscillation energy; ω is the oscillation frequency.

The internal friction or mechanical dumping of system describes by a loss factor which is defined by:

* Corresponding author. Physico-Technological Institute of Metals and Alloys, National Academy of Sciences of Ukraine, 34/1, Vernadsky Ave., Kyiv-142, 03680, Ukraine.
E-mail address: ruslan@ptima.kiev.ua (R.A. Sergiienko).

https://doi.org/10.1016/j.jallcom.2019.03.270
0925-8388/

$$\tan\delta = E^{II}(\omega)/E^{I}(\omega) \quad (2)$$

The high tan δ is typical for materials with a large portion of plastic deformation. All these parameters (E^I, E^{II}, tan δ) are related to the atomic mobility in a material and provide an opportunity to explore the features of the structure formation and crystallization of amorphous alloys. Thus, DMA analysis makes it possible to determine the parameters E^I, E^{II}, tan δ depending on time, temperature, load and frequency.

2. Experimental procedure

The ingot of the $Zr_{55}Cu_{30}Al_{10}Ni_5$ alloy (composition are given in nominal atomic percentages) has been prepared by arc melting mixtures of Zr 99.9 mass %, Cu 99.99 mass %, Al 99.9 mass %, Ni 99.9 mass % purities in an argon atmosphere. After remelting of this ingot in a vacuum induction furnace the bulk amorphous alloy rods 2 mm in diameter were prepared by the copper mould casting technique. The chemical composition of the alloy (Zr 57.52 at.%, Cu 27.21 at.%, Al 11.24 at.%, Ni 4.58 at.%) has been verified with energy-dispersive X-ray (EDX) analysis is slightly different from the nominal. The EDX spectrometer was attached to the scanning electron microscope (JEOL, JSM-6400).

Thermophysical properties were investigated by the method of differential scanning calorimetry on the STA 449F1 instrument of the German firm NETZSCH and by the method of dynamic mechanical analysis on the DMA 242C instrument of the same firm.

The rod specimen for dynamic thermomechanical measurements had dimensions of 20 mm in length and 2 mm in diameter. The specimen was subjected to a single-arm bending with maximum strain amplitude of 50 μm under controlled dynamic stress of 5 N and static stress of 0.5 N at a constant frequency of 1 Hz. The measurements of the dynamic properties (E^I, tan δ) were also performed vs. temperature at a constant heating rate of 2 K/min.

The glass transition temperature (T_g), the crystallization temperature (T_x) and the crystallization enthalpy (ΔH_x) as well as the melting point (solidus temperature T_{sol}), the solidification point (liquidus temperature T_{liq}), melting heat (ΔH_m) and solidification heat (ΔH_{sol}) were determined by using differential scanning calorimetry method. The onset temperatures of T_g and T_x were determined at the intersection of two tangent lines on the DSC curves, as shown in Fig. 1a and b. The activation energy (E_a) of the transition from an amorphous into a crystalline state was determined using the standard Kissinger analysis [10]; to do this, the amorphous samples were heated at different rates V_i (2, 5, 10, 20 K/min) and the crystallization peak temperatures (T_{xp}) in the DSC curves were determined. The experiments were carried out in a dynamic argon atmosphere at a constant flow rate of 40 ml/min. To achieve a maximum sensitivity of the DSC measurements, a special procedure of measuring and processing data was developed. It consists of two successive heating and cooling cycles without removing the sample from the crucible, and then the second heating curve was subtracted from the first heating curve. After crystallization of the amorphous sample, the caloriferic effects are absent at the second heating therefore the crystallized sample is the ideal standard for the original amorphous sample. This procedure allows increasing the sensitivity of the DSC analysis.

The phase composition of the studied alloy after heating above the crystallization temperature (T_x) was investigated by X-ray diffraction (XRD; Bruker AXS D8 Advance instrument) with θ - 2θ Bragg-Brentano geometry in monochromatic Cu-Kα (wavelength: 0.15406 nm) radiation. The X-ray diffractogram was taken in the 2θ range of 5-100° with a step width of 0.02° and scanning speed of 1.77°/min. Accelerating voltage was 40 kV at a current of 40 mA.

3. Results and discussion

3.1. Study of thermal characteristics of the $Zr_{55}Cu_{30}Al_{10}Ni_5$ bulk amorphous alloy sample

The results of the DSC studies are shown in Figs. 1–3 and given in Table 1. Fig. 1 shows the DSC curves for the studied $Zr_{55}Cu_{30}Al_{10}Ni_5$ alloy at different heating rates. The temperatures of glass transition and crystallization (Fig. 1a) were determined at different heating rates of 5 K/min, 10 K/min and 20 K/min. It was not possible to determine the glass transition temperature at a heating rate of 2 K/min due to minor change in the heat capacity with time. The DSC curves demonstrate an increment of the heat capacity at the glass transition temperature due to a significant change in the dynamic viscosity and the transition of amorphous alloy to a superplastic state. The glass transition temperature corresponds to the beginning of devitrification of the glassy phase. On further heating a subsequent sharp single exothermic peak due to crystallization of the supercooled liquid starts at the onset temperature (T_x) and transition into a crystalline state is monitored by using heat release. A wide peak with apex at the temperature of about 908 K is clearly detected on the DSC curve at a maximum heating rate of 20 K/min (Fig. 1b).

As a rule, for bulk amorphous alloys the glass transition temperature is lower than the crystallization temperature and the difference $\Delta T_x = T_x - T_g$ determines the superplasticity range. Thus, the crystallization onset temperature of the $Zr_{55}Cu_{30}Al_{10}Ni_5$ bulk amorphous alloy is well above the glass transition temperature and at the heating rates of 10 K/min, 20 K/min the superplasticity ranges (ΔT_x) are equal to 68 K, 66 K, respectively. This finding makes it possible to choose heat treatment schedules and to produce materials with a given content of microcrystalline or nanocrystalline components in an amorphous matrix. It should be noted that the glass transition and crystallization temperatures are variable quantities and depend substantially on the heating rate and with increasing heating rate they shift to higher temperatures (Table 1, Fig. 1a). This dependence has a logarithmic character as shown in Fig. 1c.

Fig. 2 shows the onset melting temperature (solidus T_{sol}) and onset solidification temperature (liquidus T_{liq}) and shaded areas for the heats of melting and solidification (ΔH_m and ΔH_{sol}) on the DSC curves and these data are presented in Table 1. The studied alloy has a wide crystallization range, and the presence of two peaks indicates an appearance of at least two phases during melting or solidification these phases.

The obtained glass transition and crystallization temperatures for the studied $Zr_{55}Cu_{30}Al_{10}Ni_5$ alloy are consistent with works, where the presented alloys of the four-component Zr-Cu-Ni-Al system have single exothermic peak [11,12]. By substituting Ag, Pd, Au or Pt for only 1 at. % Cu [13], or Ti for about 3 at.% Zr [14] the main exothermic peak becomes broader and splits into more than two peaks. The additional elements have a weak or positive mixing enthalpy with one of the constitutional elements in Zr-Al-Ni-Cu glassy alloys [13].

The value of the activation energy of the transition from an amorphous into a crystalline state was determined by the Kissinger method based on the well-known equation:

$$\ln\left(V_i/(T_{xp})^2\right) = -E_2/RT_{xp} + C \quad (3)$$

where E_a is the activation energy (J/mol); R is the universal gas constant (J/(mol K)); T_{xp} is the crystallization peak temperature (K)

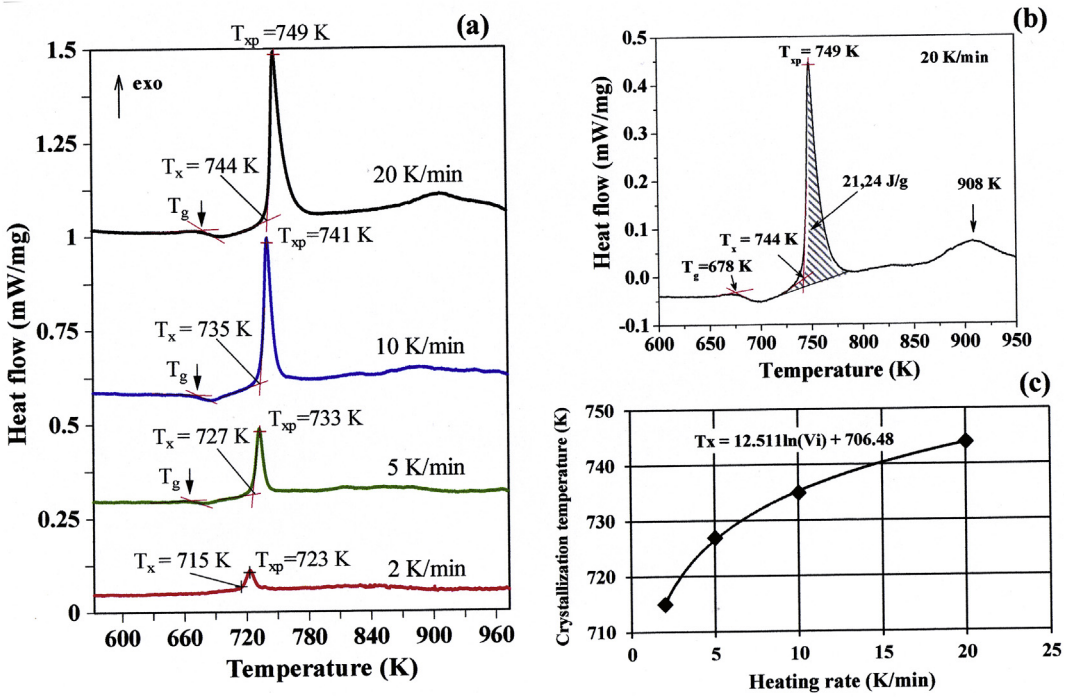

Fig. 1. (a), (b) The DSC curves of the studied $Zr_{55}Cu_{30}Al_{10}Ni_5$ amorphous alloy at different heating rates; (c) The effect of heating rate on the crystallization onset temperature (T_x) of the studied bulk amorphous alloy. The different glass transition temperatures (T_g) are marked in the Fig. 1a with arrows.

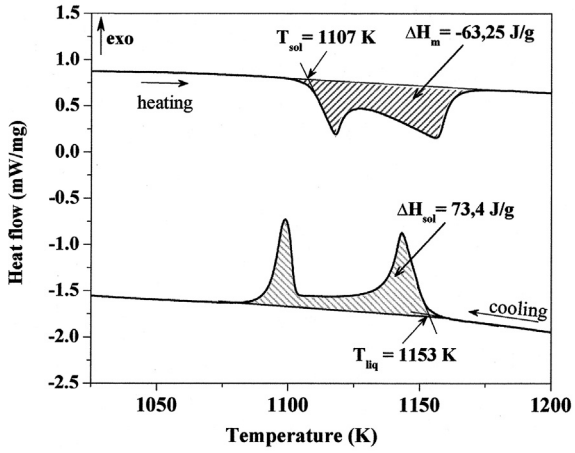

Fig. 2. The DSC curves of melting and solidification of the studied $Zr_{55}Cu_{30}Al_{10}Ni_5$ alloy at heating rate of 20 K/min.

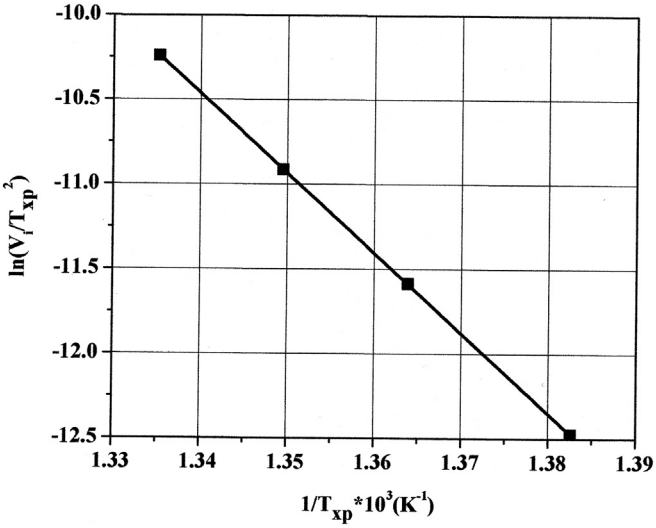

Fig. 3. Logarithmic plot for determination of the activation energy crystallization of the studied $Zr_{55}Cu_{30}Al_{10}Ni_5$ alloy using Kissinger method.

for the i-th heating rate V_i (K/min); C is the constant. With this method, the E_a is determined from the slope of the linear dependence $\ln(V_i/(T_{xp})^2) = f(1/T_{xp})$ (Fig. 3) obtained for a series of experiments performed at different heating rates:

$$E_a = -tg\varphi \cdot R \quad (4)$$

And for the studied alloy, the value of E_a is equal to 393 kJ/mol.

3.2. Study of crystallization of the $Zr_{55}Cu_{30}Al_{10}Ni_5$ bulk amorphous alloy sample by DMA method

Based on the fact [7] that the dynamic mechanical properties are more sensitive to the structure evolution, the DMA method was used to study the variation in storage modulus (E^I) and loss factor ($\tan\delta$) during continuous heating under loading. In order to enhance a direct comparison, the curve corresponding to E^I was normalized using the room temperature value of storage modulus (E^I_{rt}); since at this temperature (302 K) the viscoelastic components (E^{II} or $\tan\delta$) are negligible. E^I_{rt} can be considered as a value of unrelaxed material. Fig. 4 shows the evolution of the normalized storage modulus (E^I/E^I_{rt} – curve 1) and the loss factor ($\tan\delta$ – curve 2) during heating at 2 K/min up to the maximum temperature of 873 K. As the normalized storage modulus and its absolute value have the same behavior on heating therefore in the following text one will simply refer to the storage modulus (E^I).

Table 1
Thermal data of the studied $Zr_{55}Cu_{30}Al_{10}Ni_5$ bulk amorphous alloy sample.

V_i (K/min)	T_g (K)	T_x (K)	$\Delta T_x = T_x - T_g$ (K)	ΔH_x (J/g)	T_{sol} (K)	T_{liq} (K)	ΔH_m (J/g)	ΔH_{sol} (J/g)
2	–	715	–					
5	664	727	63					
10	667	735	68					
20	678	744	66	21.24	1107	1153	- 63.25	73.4

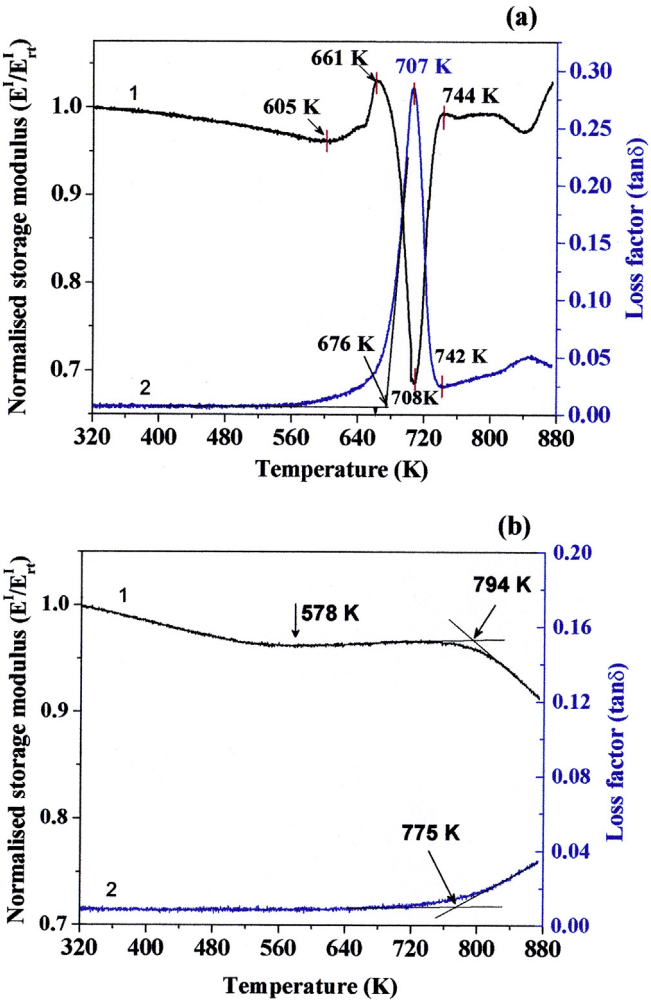

Fig. 4. The temperature dependence of the normalized storage modulus (E^I/E^I_{rt} – curve 1) and loss factor (tan δ – curve 2) during successive heating up: (a) the first heating shows the transition of the $Zr_{55}Cu_{30}Al_{10}Ni_5$ alloy sample from an amorphous into a crystalline state; (b) the second heating of the sample in the crystalline state. Frequency: 1 Hz. Heating rate: 2 K/min.

The storage modulus (E^I – curve 1, Fig. 4a) slightly decreases on heating from room temperature to 605 K, and the loss factor (tan δ – curve 2, Fig. 4a) remains unchanged with increasing temperature up to 573 K. Thus, after heating up to 605 K the only evolution observed is structural relaxation and the sample is still fully amorphous and behaves like an elastic material with loss factor almost equals to zero. Further increase in temperature from 605 K begins with progressive increase of E^I and its value reaches maximum at a temperature of 661 K. The simultaneous growth of the storage modulus and the loss factor in temperature range from 605 K to 661 K is not clear and obviously associated with the start of structural changes in the material; the nature of this phenomenon should be studied in the future.

The loss factor (tan δ) increases drastically starting with a temperature of 676 K (onset of the rising in curve 2, Fig. 4a) and reaches its maximum at a temperature of 707 K. At the same time, the storage modulus (E^I) decreases sharply from the temperature of 661 K to its minimum value at 708 K (curve 1, Fig. 4a). Most probably the temperature of 661 K is close to the glass transition temperature (T_g) at a heating rate of 2 K/min. In the superplasticity range (ΔT_x) the atomic mobility is large, so above the temperature of 661 K the storage modulus decreases significantly and the loss factor exhibits a large increase and the alloy behaves like a plastic material (i.e. the proportion of plastic deformation increases). One can see similarities with such a mechanical behavior reported for other bulk metallic glasses [7,15]. DMA measurements were correlated with the results obtained by using DSC method. The glass transition temperature $T_g = 664$ K measured by DSC method at 5 K/min (Table 1, Fig. 1a) is larger than the temperature $T_g = 661$ K estimated at 2 K/min by DMA method, since a greater T_g corresponds to a greater value of heating rate (V_i). The onset of crystallization at a heating rate of 2 K/min determined by using DSC method equals to $T_x = 715$ K (Fig. 1a) and this value is close to the minimum temperature of 708 K shown in the DMA curve 1 (Fig. 4a). On further heating the alloy starts to crystallize and elastic properties of the material increase, therefore tan δ shows a significant drop to a minimum temperature of 742 K (curve 2, Fig. 4a) while E^I grows rapidly and reaches its maximum at 744 K (curve 1, Fig. 4a). One must remember that it is necessary to compare the measurement results obtained by different methods at the same heating rate, i.e. at 2 K/min.

Irreversible changes are induced by heating above the crystallization temperature, since the sample becomes crystalline. Large differences exist between heating routes for E^I and tan δ presented in Fig. 4a and b. Fig. 4b shows the change of storage modulus and loss factor for the crystalline sample. At a temperature of 578 K the value of storage modulus (E^I – curve 1, Fig. 4 b) is 4% down from its value at room temperature, and then E^I rises about half a percent to a temperature of 730 K. Above the temperature of 794 K, a progressive decrease of E^I are observed, that is, the material loses its elastic properties. The loss factor is not changed during continuous heating from room temperature to 720 K (tan δ – curve 2, Fig. 4 b), and then tan δ begins to increase steeply above the temperature of 775 K as the material plasticity increases.

Thus, DMA studies have shown that at temperatures below the glass transition temperature (T_g) the structural relaxation are occurred in amorphous material and the storage modulus and loss factor vary insignificantly. At temperatures above the glass transition temperature in the superplasticity range (ΔT_x) an atomic mobility is significantly increased and above the crystallization temperature (T_x) the sample crystallizes therefore the storage modulus and loss factor are changed drastically.

3.3. The crystalline structure of the studied $Zr_{55}Cu_{30}Al_{10}Ni_5$ alloy sample

A large number of dark inclusions (Fig. 5) with a submicroscopic size of less than 0.5 μm have been developed in the structure of the alloy sample after heating above the crystallization temperature. By

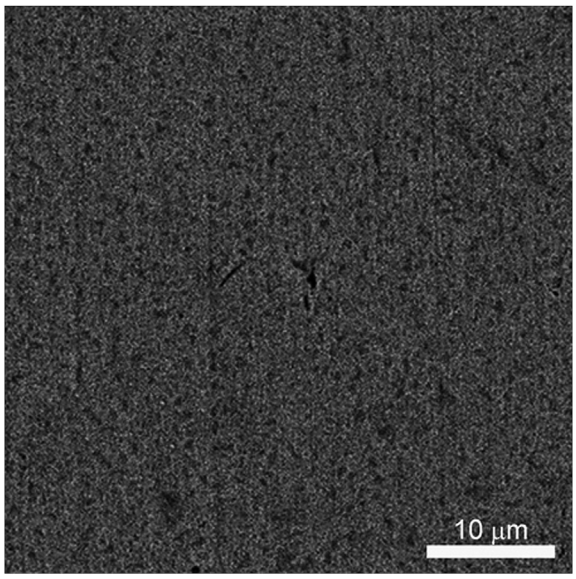

Fig. 5. The scanning electron microscopy image of the studied $Zr_{55}Cu_{30}Al_{10}Ni_5$ alloy sample after heating above the crystallization temperature (T_x).

comparing the observed X-ray diffraction reflections with reference X-ray powder diffractograms (Fig. 6) it can be concluded that the crystal structure of the studied $Zr_{55}Cu_{30}Al_{10}Ni_5$ alloy sample after crystallization consists of several phases: 1) the body-centered tetragonal *tI6* Zr_2Cu phase with the space group *I*4/*mmm*; 2) the possible presence of the face-centered cubic *cF116* $Zr_6Ni_8Al_{15}$ (or FCC $Al_5Ni_3Zr_2$) phase with the space group *Fm3m*; 3) the diffraction peaks from an unknown phase. The calculated lattice parameters of

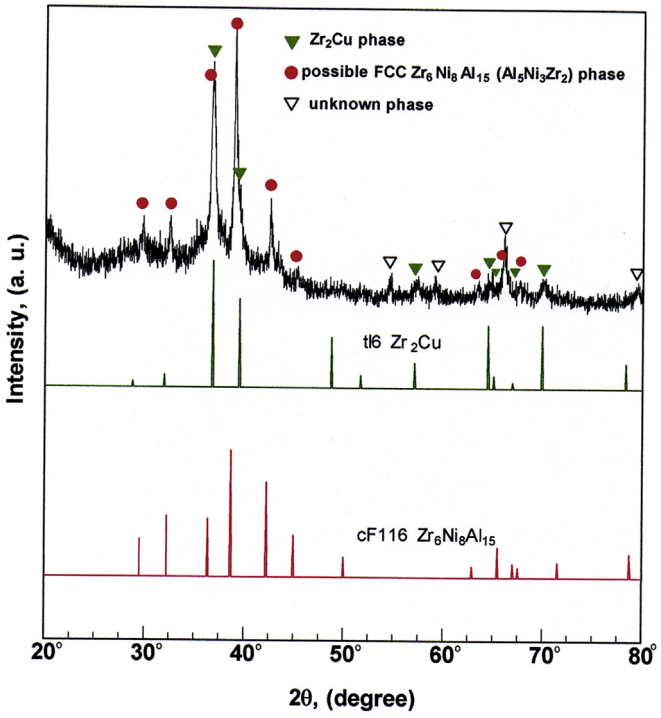

Fig. 6. The X-ray diffractogram of the studied $Zr_{55}Cu_{30}Al_{10}Ni_5$ alloy sample after heating above the crystallization temperature (T_x) and the reference powder diffractograms of *tI6* Zr_2Cu and *cF116* $Zr_6Ni_8Al_{15}$ phases taken from Inorganic Material Database of NIMS.

the *tI6* Zr_2Cu phase in the studied $Zr_{55}Cu_{30}Al_{10}Ni_5$ alloy sample are $a = 0.32237 \pm 0.001$ nm, $c = 1.11957 \pm 0.009$ nm ($P = 0.95$) and the reference unit cell parameters taken from JCPDS powder diffraction file № 18-0466 are $a = 0.322$ нм, $c = 1.118$ nm. The formation of several crystalline phases by a single-stage reaction argues for an eutectic-like reaction and the main crystallization process was governed by three-dimensional growth at increasing nucleation rate [16].[1]

The *tI6* Zr_2Cu phase was often observed in other research works after crystallization of amorphous cylindrical rods, ribbons [14,17–20], samples of a rectangular cross-section [21], and in the deposited layers of Zr-based bulk metallic glass [22]. The presence of *tI6* Zr_2Cu phase has been reported at 773 K in the computed isothermal section the Al-Cu-Zr phase diagram in work [23] and a large volume fraction (>50%) of the Zr_2Cu phase has been confirmed by calculation of phase composition using the Thermo-Calc software. According to the ternary diagram [23], in addition to the *tI6* Zr_2Cu phase in the composition area of the $Zr_{55}Cu_{30}Al_{10}Ni_5$ alloy other phases are depicted – *oS68* $Cu_{10}Zr_7$ and ternary (ZrCuAl) τ_2, τ_3 phases with an unknown structure.

cF116 $Zr_6Ni_8Al_{15}$ (FCC $Al_5Ni_3Zr_2$, $a = 1.203$ nm) phase was detected by X-ray and electron diffractions in work [22] for the $Zr_{55}Cu_{30}Al_{10}Ni_5$ BMGs deposit prepared by laser solid forming. The faceted FCC $Al_5Ni_3Zr_2$ phase was sparsely distributed on the dendritic-like eutectic *tI6* Zr_2Cu phase [22]. In our work, in the crystal structure of the studied $Zr_{55}Cu_{30}Al_{10}Ni_5$ alloy, the presence of ternary phase with the same composition and structure *cF116* $Zr_6Ni_8Al_{15}$ (FCC $Al_5Ni_3Zr_2$) is also possible.

4. Conclusions

In this work, the transition process from an amorphous into a crystalline state has been investigated for the $Zr_{55}Cu_{30}Al_{10}Ni_5$ bulk amorphous alloy by the differential scanning calorimetry and the dynamic mechanical analysis. Based on the results of DSC studies, it has been shown that the values of the glass transition and crystallization temperatures are shifted to higher temperatures with an increase in the heating rate. The crystallization temperature dependence of the heating rate is given by the logarithmic relationship.

The DMA method in comparison with DSC method is more sensitive to the structure changes that occur during the heat treatment of the amorphous alloy sample. From character of the storage modulus (E^I) and the loss factor ($\tan\delta$) behavior one can judge the change in the elastic and plastic properties of the material during heating. It has been established that at temperatures below the glass transition temperature, structural relaxation occurs in the material, which is characterized by insignificant changes in the storage modulus and the loss factor. The parameters E^I, $\tan\delta$ are changed drastically at temperatures above T_g in the superplasticity range (ΔT_x) with increase of an atomic mobility in the material and above T_x due to crystallization of amorphous alloy. The temperature dependences of E^I and $\tan\delta$ for the crystalline reheated sample are significantly different from the original amorphous sample.

X-ray analysis showed that crystallization of the original amorphous alloy sample mainly resulted in several phases – tetragonal body-centered *tI6* Zr_2Cu, face-centered cubic *cF116* $Zr_6Ni_8Al_{15}$ (FCC $Al_5Ni_3Zr_2$) and a small fraction of an unidentified phase.

[1] https://crystdb.nims.go.jp/index_en.html.

Acknowledgement

The authors gratefully acknowledge the financial support of the Ministry of Education and Science of the Russian Federation in the framework of Increase Competitiveness Program of NUST « MISiS» (№ К3-2018-019). Additional support through the European Research Council under the ERC Advanced Grant INTELHYB, grant number: ERC-2013-ADG-340025.

References

[1] A. Inoue, High strength bulk amorphous alloys with low critical cooling rates (*Overview*), Mater. Trans., JIM 36 (7) (1995) 866–875. https://www.jim.or.jp/journal/e/36/07/866.html.

[2] A. Inoue, X.M. Wang, W. Zhang, Developments and applications of bulk metallic glasses, Rev. Adv. Mater. Sci. 18 (2008) 1–9. http://www.ipme.ru/e-journals/RAMS/no_11808/inoue.pdf.

[3] A. Inoue, Stabilization of metallic supercooled liquid and bulk amorphous alloys, Acta Mater. 48 (2000) 279–306. https://doi.org/10.1016/S1359-6454(99)00300-6.

[4] O.A. Shcheretskyy, V.L. Lakhnenko, V.S. Shumikhin, A.A. Bespalyy, A.V. Soloviova, Fabrication of nanostructural materials by means of heat-treatment of amorphous $Zr_{64}Cu_{16}Ni_{10}$ $Al_{9.5}Nb_{0.5}$ alloy, Metallofiz. Noveishie Tekhnol. 33 (10) (2011) 1323–1332 (in Russian), https://doi.org/10.15407/mfint.

[5] S. Shumikhin, A.A. Shcheretskiy, V.L. Lakhnenko, A.A. Bespalyy, Cast composite materials with amorphous matrix based on Zirconium, Nanosystemy, nanomaterialy, nanotekhnolohii – nanosystems, nanomaterials, Nanotechnologies 7 (3) (2009) 901–909 (in Russian), https://www.imp.kiev.ua/nanosys/media/pdf/2009/3/nano_vol7_iss3_p0901p0909_2009.pdf.

[6] A. Inoue, T. Zhang, J. Saida, M. Matsushita, M.W. Chen, T. Sakurai, High strength and good ductility of bulk quasicrystalline base alloys in $Zr_{65}Al_{7.5}Ni_{10}Cu_{17.5-x}Pd_x$ system, Mater. Trans., JIM 40 (10) (1999) 1137–1143. https://www.jim.or.jp/journal/e/40/10/1137.html.

[7] J.-M. Pelletier, D.V. Louzguine-Luzgin, S. Li, A. Inoue, Elastic and viscoelastic properties of glassy, quasicrystalline and crystalline phases in $Zr_{65}Cu_5Ni_{10}Al_{7.5}Pd_{12.5}$ alloys, Acta Mater. 59 (2011) 2797–2806. https://doi.org/10.1016/j.actamat.2011.01.018.

[8] A.V. Soloviova, A.A. Shcheretskiy, Prigotovlenie nanostrukturnyih materialov na osnove tsirkoniya s zadannyim urovnem uprugih svoystv [Preparation of nanostructured materials based on zirconium with a given level of elastic properties], Protsessyi Litya – Casting Processes 1 (97) (2013) 65. http://dspace.nbuv.gov.ua/bitstream/handle/123456789/131124/14-Solovieva.pdf?sequence=1.

[9] Kevin P. Menard, Dynamic Mechanical Analysis: a Practical Introduction, second ed., CRC Press, 2008.

[10] H.E. Kissinger, Variation of peak temperature with heating rate in differential thermal analysis, J. Res. Natl. Bur. Stand. (J. Res. Natl. Inst. Stan.) 57 (4) (1956) 217–220. https://doi.org/10.6028/jres.057.026.

[11] M. Stoica, N. Van Steenberge, J. Bednarčik, N. Mattern, H. Franz, J. Eckert, Changes in short-range order of $Zr_{55}Cu_{30}Al_{10}Ni_5$ and $Zr_{55}Cu_{20}Al_{10}Ni_{10}Ti_5$ BMGs upon annealing, J. Alloys Compd. 506 (2010) 85–87. https://doi.org/10.1016/j.jallcom.2010.07.001.

[12] K. Chai, T. Lin, P. He, J. Sun, The limited annealing treatment of the $Zr_{55}Cu_{30}Al_{10}Ni_5$ metallic glass below its glass transition temperature, J. Alloys Compd. 620 (2015) 137–141. https://doi.org/10.1016/j.jallcom.2014.09.122.

[13] J. Saida, M. Matsushita, A. Inoue, Stability of supercooled liquid and transformation behavior in Zr-based glassy alloys, Mater. Trans., JIM 43 (8) (2002) 1937–1946. https://www.jim.or.jp/journal/e/43/08/1937.html.

[14] L.Q. Xing, T.C. Hufnagel, J. Eckert, W. Löser, L. Schultz, Relation between short-range order and crystallization behavior in Zr-based amorphous alloys, Appl. Phys. Lett. 77 (13) (2000) 1970–1972. https://doi.org/10.1063/1.1313255.

[15] J.-M. Pelletier, Y. Yokoyama, A. Inoue, Dynamic mechanical properties in a $Zr_{50}Cu_{40}Al_{10}$ bulk metallic glass, Mater. Trans., JIM 48 (6) (2007) 1359–1362. https://www.jim.or.jp/journal/e/48/06/1359.html.

[16] L. Liu, Z.F. Wu, J. Zhang, Crystallization kinetics of $Zr_{55}Cu_{30}Al_{10}Ni_5$ bulk amorphous alloy, J. Alloys Compd. 339 (2002) 90–95. https://doi.org/10.1016/S0925-8388(01)01977-6.

[17] D.V. Louzguine-Luzgin, C. Suryanarayana, T. Saito, Q. Zhang, Na Chen, J. Saida, A. Inoue, Unusual solidification behavior of a Zr-Cu-Ni-Al bulk glassy alloy made from low-purity Zr, Intermetallics 18 (2010) 1531–1536. https://doi.org/10.1016/j.intermet.2010.04.003.

[18] T. Fukami, K. Okabe, D. Okai, T. Yamasaki, T. Zhang, A. Inoue, Crystal growth and time evolution in Zr-Al-Cu-Ni glassy metals in supercooled liquid, Mater. Sci. Eng. B 111 (2004) 189–196. https://doi.org/10.1016/j.mseb.2004.04.020.

[19] D.V. Louzguine-Luzgin, G. Xie, Q. Zhang, A. Inoue, Effect of Fe on the glass-forming ability, structure and devitrification behavior of Zr-Cu-Al bulk glass-forming alloys, Philos. Mag. 90 (14) (2010) 1955–1968. https://doi.org/10.1080/14786430903571495.

[20] D.V. Louzguine-Luzgin, G.Q. Xie, S. Gonzales, J.Q. Wang, K. Nakayama, J.H. Perepezko, A. Inoue, Nano-crystallization behavior of Zr-Cu-Al bulk glass-forming alloy, J. Non-Cryst. Solids 358 (2012) 145–149. https://doi.org/10.1016/j.jnoncrysol.2011.08.026.

[21] A.R. Yavari, A. Le Moulec, W.J. Botta, A. Inoue, P. Rejmankova, A. Kvick, In situ crystallization of $Zr_{55}Cu_{30}Al_{10}Ni_5$ bulk glass forming from the glassy and undercooled liquid states using synchrotron radiation, J. Non-Cryst. Solids 247 (1999) 31–34. https://doi.org/10.1016/S0022-3093(99)00027-7.

[22] X. Lin, Y. Zhang, G. Yang, X. Gao, Q. Hu, J. Yu, L. Wei, W. Huang, Microstructure and compressive/tensile characteristic of large size Zr-based bulk metallic glass prepared by laser solid forming, Mater. Sci. Technol. 35 (2) (2019) 328–335. https://doi.org/10.1016/j.jmst.2018.10.033.

[23] V. Raghavan, Al-Cu-Zr (Aluminum-Copper-Zirconium), J. Phase Equilibria Diffusion 32 (2011) 452–454. https://doi.org/10.1007/s11669-011-9920-z.